

Full spatial characterization of entangled structured photons

Xiaoqin Gao,¹ Yingwen Zhang,^{1,2} Alessio D’Errico,¹ Alicia Sit,¹ Khabat Heshami,^{2,1} and Ebrahim Karimi^{1,2}

¹*Nexus for Quantum Technologies, University of Ottawa, K1N 5N6, Ottawa, ON, Canada*

²*National Research Council of Canada, 100 Sussex Drive, K1A 0R6, Ottawa, ON, Canada*

(Dated: April 28, 2023)

Vector beams (VBs) are fully polarized beams with spatially varying polarization distributions, and they have found widespread use in numerous applications such as microscopy, metrology, optical trapping, nano-photonics, and communications. The entanglement of such beams has attracted significant interest, and it has been shown to have tremendous potential in expanding existing applications and enabling new ones. However, due to the complex spatially varying polarization structure of entangled VBs (EVBs), a complete entanglement characterization of these beams remains challenging and time-consuming. Here, we have used a time-tagging event camera to demonstrate the ability to simultaneously characterize approximately 2.6×10^6 modes between a bi-partite EVB using only 16 measurements. This achievement is an important milestone in high-dimensional entanglement characterization of structured light, and it could significantly impact the implementation of related quantum technologies. The potential applications of this technique are extensive, and it could pave the way for advancements in quantum communication, quantum imaging, and other areas where structured entangled photons play a crucial role.

INTRODUCTION

Quantum entanglement [1] is a remarkable feature of quantum theory that has become a cornerstone in photonic quantum information processing, encompassing quantum computation [2], quantum teleportation [3], quantum cryptography [4], and quantum dense coding [5]. Demonstrated across various degrees of freedom, including polarization [6], orbital angular momentum [7, 8], path [9], and time-bin [10], photonic entanglement has gained prominence as technologies leveraging it become more integrated into daily life. Consequently, examining intricate entanglement structures and their applications is increasingly vital.

Distinct from homogeneously polarized light, vector beams (VBs) display a complex, spatially varying polarization structure [11]. Owing to their unique attributes, VBs have recently attracted attention in diverse fields such as nonlinear optics [12], high-resolution imaging [13], laser processing [14], classical or quantum communication [15–17], sharper focus spots [18, 19], and quantum key distribution [20, 21]. Two primary approaches to generate VBs include the intra-cavity method, which involves inserting mode-selection optical elements in a laser resonator [22–24], and the extra-cavity method, which entails transforming Gaussian beams into VBs using specialized optical elements like q -plates [25, 26] or a spatial light modulator combined with a Sagnac interferometer [27].

Entangled VBs (EVBs) have been demonstrated in [28, 29], where polarization-entangled photon pairs are converted into VBs, transforming spatially homogeneous polarization entanglement into a complex, spatially variant polarization entanglement structure. However, thoroughly characterizing this spatially dependent entanglement is challenging. Employing single-pixel detectors,

such as avalanche photodiodes, necessitates $(N \times N)^2 \times 16$ measurements, with $N \times N$ representing the number of spatial locations on each beam to be probed, and 16 denoting the required polarization measurement combinations [30]. By using a triggerable intensified CCD (ICCD) camera, where a single-pixel detector triggers the ICCD, the number of measurements can be reduced to $(N \times N) \times 16$, as partially demonstrated in the case of a homogeneously polarized beam entangled to a VB [27, 31].

Here, we present the full characterization of spatially dependent polarization entanglement between EVBs using only 16 polarization measurements, facilitated by a time-tagging event camera. Covering approximately 40×40 pixels per beam, $\sim 2.6 \times 10^6$ modes between a bi-partite entangled state are measured simultaneously. To showcase the versatility of our technique, we perform the characterization for various polarization topological patterns, including vector-vortex, lemon, star, and spiral polarization patterns, all exhibiting exceptional agreement with the anticipated entanglement pattern derived from theory.

RESULTS

Theory: The conceptual diagram for the generation and characterization of spatially varying polarisation entangled photons is shown in Fig. 1. A polarization-entangled state with a Gaussian beam profile of the following form is first prepared,

$$|\Psi_0\rangle = \frac{1}{\sqrt{2}} (|H, V\rangle - |V, H\rangle) = \frac{i}{\sqrt{2}} (|L, R\rangle - |R, L\rangle), \quad (1)$$

where $|L, R\rangle = |L\rangle_s \otimes |R\rangle_i$ with $|L\rangle$ and $|R\rangle$ denoting left- and right-circular polarization, and the subscripts s and

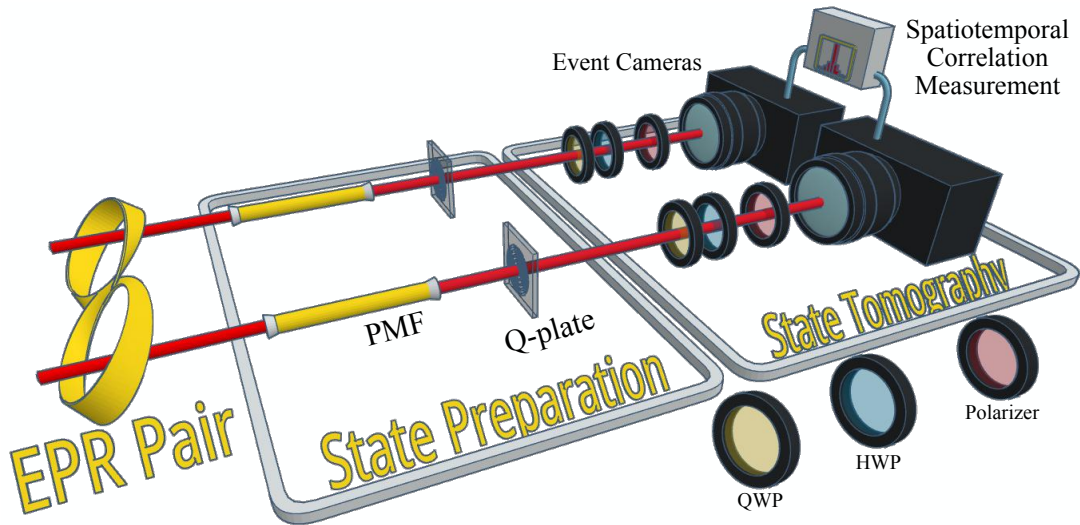


FIG. 1. **Conceptual setup for the generation and characterization of vector beam entanglement.** Einstein–Podolsky–Rosen (EPR) photon pairs entangled in the polarization degree of freedom are first spatially filtered by polarization-maintaining single-mode fibres (PMF) into the fundamental mode before being sent onto the q -plates (with different topological charges) to create entangled structured photons. Polarization state tomography is performed using a combination of quarter-wave plates (QWP), half-wave plates (HWP), and polarizers with the photon pairs detected by time-tagging event cameras from which spatial-temporal information of the photons is collected. A spatial-temporal correlation measurement is then performed for each of the 16 combinations of polarization measurement. The density matrix and, subsequently, the Bell states for each pixel combination can then be determined.

i denoting the signal and idler photons, respectively.

The unitary action of a q -plate with topological charge q acting on a circularly polarized Gaussian beam can be written as [32],

$$\hat{U}_q^\delta \cdot \begin{bmatrix} |L\rangle \\ |R\rangle \end{bmatrix} = F_0(r) \cos\left(\frac{\delta}{2}\right) \begin{bmatrix} |L\rangle \\ |R\rangle \end{bmatrix} + i \sin\left(\frac{\delta}{2}\right) F_q(r) \begin{bmatrix} e^{-i2q\theta} |R\rangle \\ e^{i2q\theta} |L\rangle \end{bmatrix}, \quad (2)$$

where $F_0(r)$ and $F_q(r)$ determine the radial profiles of the unconverted and converted beams, respectively – here, we considered q -plates wherein the local optical axis distribution of the liquid crystals is $\alpha(\theta) = q\theta$. Both $F_0(r)$ and $F_q(r)$ can be expressed analytically in terms of hypergeometric Gauss modes [33]. However, for q -plates with low q values, within a good approximation, both radial functions can be expressed in terms of the Laguerre-Gauss modes possessing azimuthal indices of 0 and $2q$, and radial index zero at $z = 0$, respectively, i.e., $F_q(r)e^{\pm i2q\theta} \equiv \text{LG}_{0,\pm 2q}(r, \theta)$ [32]. $\delta \in [0, \pi]$ is the optical retardation of the q -plate, which can be tuned based on the voltage applied to the q -plates [34]. Therefore, sending each photon onto different q -plates yields the following complex space-varying polarization-entangled state,

$$|\Psi_f\rangle = \frac{1}{\sqrt{2}} \left(\hat{U}_{q_s}^{\delta_s} \cdot |L\rangle_s \hat{U}_{q_i}^{\delta_i} \cdot |R\rangle_i - \hat{U}_{q_s}^{\delta_s} \cdot |R\rangle_s \hat{U}_{q_i}^{\delta_i} \cdot |L\rangle_i \right), \quad (3)$$

here, $\hat{U}_{q_s}^{\delta_s}$ and $\hat{U}_{q_i}^{\delta_i}$ denotes the signal and idler q -plate actions, respectively – note that the global $U(1)$ -phase

of $\pi/2$ is omitted. The four parameters of $\{q_s, \delta_s, q_i, \delta_i\}$ determine the polarization entanglement state between signal and idler photons. For instance, setting $q_s = q_i = 1/2$ and $\delta_s = \delta_i = \pi/2$, the polarization Einstein–Podolsky–Rosen (EPR) state is transformed into the radial and azimuthal entangled state, i.e., $(|\text{radial}, \text{azimuthal}\rangle - |\text{azimuthal}, \text{radial}\rangle) / \sqrt{2}$. To characterize the spatially varying entanglement between the entangled photons, polarization state tomography is performed using 16 different combinations of polarization measurement. Each photon is then collected by a time-tagging event camera from which spatial-temporal information about the photons is recorded. A spatial-temporal correlation measurement is then performed between the two cameras for each of the 16 polarization measurements from which the spatially varying density matrix and, subsequently, the Bell states contributions can be determined.

Experimental Results: In this work, we demonstrate the entanglement characterization for two q -plate settings: the case of when both q -plates are perfectly tuned ($\delta_s = \delta_i = \pi$) and when both are partially tuned ($\delta_s = \delta_i = \pi/2$). For two tuned q -plates with topological charges q_s and q_i applied to the signal and idler photons, respectively, the transverse position-dependent polarization entanglement between the EVBs can be decomposed into the four Bell states, $|\phi^\pm\rangle = \frac{1}{\sqrt{2}}(|H\rangle_s |H\rangle_i \pm |V\rangle_s |V\rangle_i)$ and $|\psi^\pm\rangle = \frac{1}{\sqrt{2}}(|H\rangle_s |V\rangle_i \pm |V\rangle_s |H\rangle_i)$, with the following

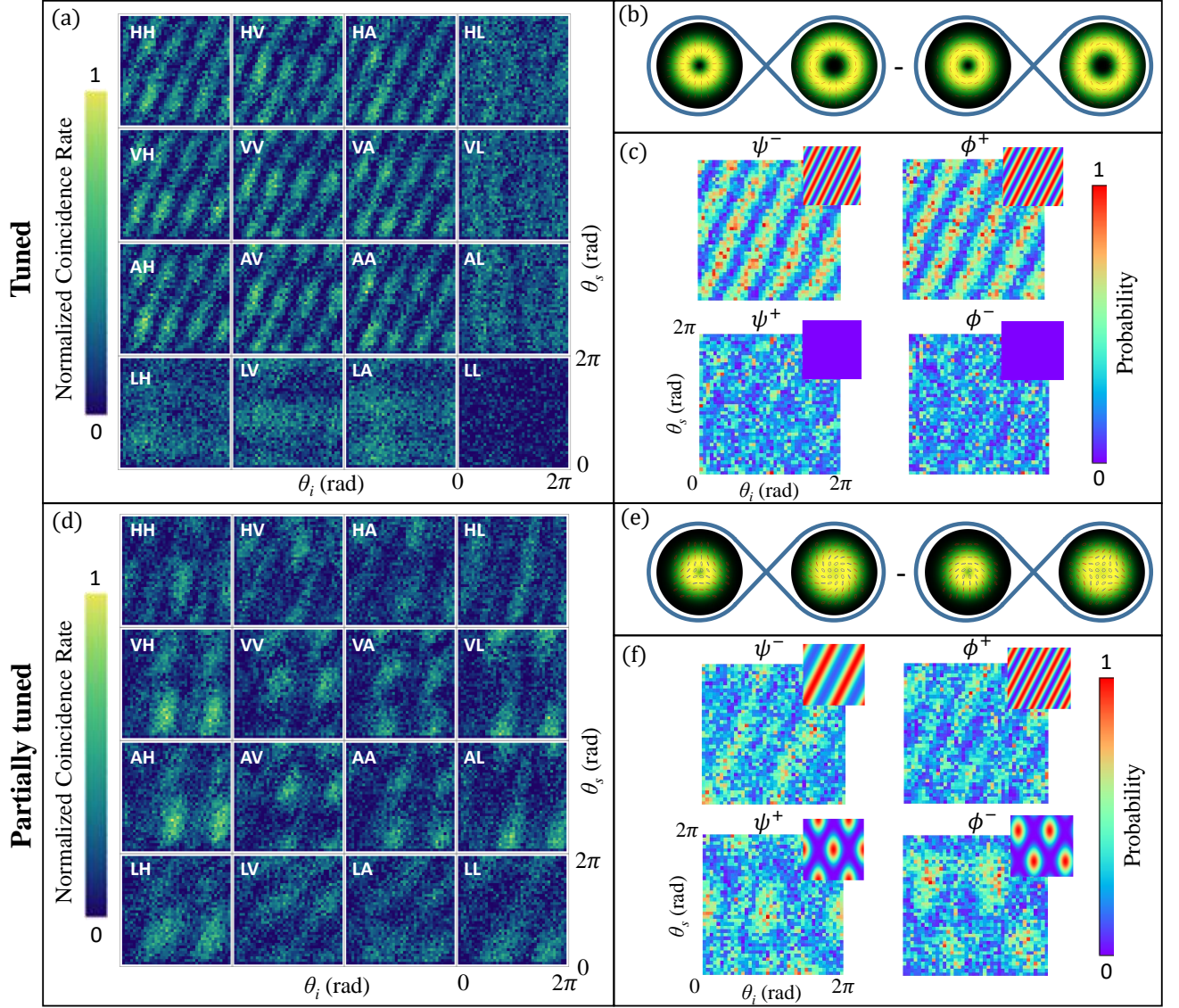


FIG. 2. Measured spatial correlations and entanglement characterization for bi-photon with spatially varying polarization states generated via two q -plates. (a) Two-photon spatial correlations between two entangled vector beams measured in the azimuthal degree of freedom from 16 different polarization measurements. Two tuned q -plates ($\delta_s = \delta_i = \pi$) with topological charges $q_i = 1$ and $q_s = 1/2$ are used to generate the entangled vector vortex photons. (b) Graphical representation of the polarization patterns overlaid on the photon probability distribution for an input EPR pair in the antisymmetric Bell state. (c) Reconstructed probabilities for the four Bell states $\{|\psi^+\rangle, |\psi^-\rangle, |\phi^+\rangle, |\phi^-\rangle\}$. The insets are the respective theoretical probabilities. (d-f) Corresponding results for two partially tuned q -plates ($\delta_s = \delta_i = \pi/2$) with topological charges $q_i = 1$ and $q_s = 1/2$. Red lines in (b) and red (blue) ellipses in (e) show the major axes of the polarization.

contributions,

$$\begin{aligned}
 P_{\phi^+}^t &= F_{q_s, q_i}^2(r_s, r_i) \sin^2 2(q_s \theta_s - q_i \theta_i), \\
 P_{\phi^-}^t &= 0, \\
 P_{\psi^+}^t &= 0, \\
 P_{\psi^-}^t &= F_{q_s, q_i}^2(r_s, r_i) \cos^2 2(q_s \theta_s - q_i \theta_i),
 \end{aligned} \tag{4}$$

where $F_{q_s, q_i}(r_s, r_i) = F_{q_s}(r_s)F_{q_i}(r_i)$, and (r_s, θ_s) and (r_i, θ_i) are the transverse coordinates of signal and idler photons. For the partially tuned case, ($\delta_s = \delta_i = \pi/2$),

the contributions are,

$$\begin{aligned}
 P_{\phi^+}^{\text{pt}} &= \frac{1}{4} F_{q_s, q_i}^2(r_s, r_i) \sin^2 2(q_s \theta_s - q_i \theta_i), \\
 P_{\phi^-}^{\text{pt}} &= \frac{1}{4} [F_{0, q_i}(r_s, r_i) \sin 2q_i \theta_i - F_{q_s, 0}(r_s, r_i) \sin 2q_s \theta_s]^2, \\
 P_{\psi^+}^{\text{pt}} &= \frac{1}{4} [F_{0, q_i}(r_s, r_i) \cos 2q_i \theta_i - F_{q_s, 0}(r_s, r_i) \cos 2q_s \theta_s]^2, \\
 P_{\psi^-}^{\text{pt}} &= \frac{1}{4} [F_{0, 0}(r_s, r_i) - F_{q_s, q_i}(r_s, r_i) \sin 2(q_s \theta_s - q_i \theta_i)]^2.
 \end{aligned} \tag{5}$$

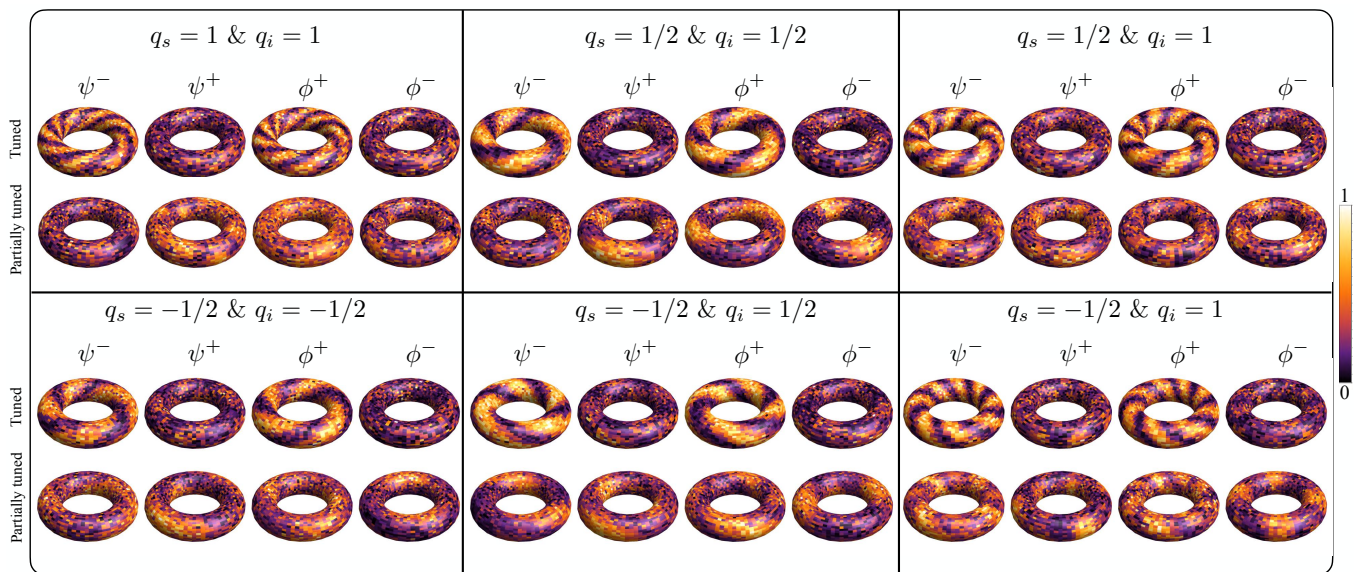


FIG. 3. **The experimental results for the probabilities of the four Bell states.** The Bell state probabilities at different azimuthal angles between the two entangled vector beams are mapped onto a torus. The vector beams are generated for a combination of q -plates with a fractional topological charge of $q = -1/2, 1/2, \text{ or } 1$ in each path.

Detailed calculations can be found in the Supplementary materials.

The Bell state contributions for EVBs generated with tuned q -plates depend only on the azimuthal degree of freedom (DOF), θ_s and θ_i , and of course, the plates, topological charges q_s, q_i , while both ϕ^- and ψ^+ states make no contributions. For partially tuned q -plates, the situation is more complex since all four Bell states make contributions. Indeed, Bell states are a function of both the azimuthal DOF, θ_s and θ_i , and the radial DOF, r_s and r_i .

In the experimental demonstration, a single time-tagging camera was employed as an alternative to the originally proposed dual-camera setup. Each beam of the EVB pair was directed towards a corner of the camera, encompassing an area of roughly 40×40 pixels. An initial temporal correlation measurement was conducted to identify photon pairs using the position and time data of each photon captured by the camera. This was followed by a spatial correlation measurement conducted in cylindrical polar coordinates. This procedure was repeated for 16 distinct polarization measurement combinations, as required for bi-photon polarization state tomography [30]. The quantum state tomography for EVBs generated with q -plates of topological charges $q_s = 1/2$ and $q_i = 1$ is illustrated in Fig. 2. The measured spatial correlation between signal and idler photons in the azimuthal DOF θ , with radial DOF r summed over, is presented for the 16 different polarization combinations employed in polarization state tomography, see Fig. 2(a). Correlations in the radial DOF exhibited minimal variation between distinct polarization measurements and are,

therefore, not depicted here, but can be found in the Supplementary materials. Subsequently, an azimuthal angle-dependent density matrix was reconstructed, and to simplify visualization, the corresponding Bell state decomposition is displayed in Fig. 2(c). We observe azimuthally that the measured Bell state contributions oscillate between the $|\psi^- \rangle$ and $|\phi^+ \rangle$ states, with negligible contributions from the $|\phi^- \rangle$ and $|\psi^+ \rangle$ states. This outcome aligns well with the theoretical calculations reported in Eq. (4). Imperfections in the q -plates, entanglement, and some noise may contribute to residual oscillations in the $|\psi^+ \rangle$ and $|\phi^- \rangle$ states. The measured concurrence, averaged over all $|\phi \rangle$, of the EVB is 0.540 ± 0.005 . Results for two partially tuned q -plates with topological charges $q_s = 1/2$ and $q_i = 1$ are displayed in Fig. 2(d-f). Due to the increased complexity of the spatially variant structure and sensitivity to optical alignment, the state tomography results are noisier, yet they still demonstrate reasonable agreement with theoretical expectations. The average concurrence of the EVB is measured to be 0.517 ± 0.005 .

Figure 3 displays the experimentally measured Bell state decomposition for EVBs generated using both tuned and partially tuned q -plates at various combinations of topological charges. The probability amplitudes of the Bell states are mapped onto a torus due to the cyclic nature of the azimuthal angle of polar coordinates (θ_s, θ_i) . For the measured spatial correlations of all q -plate combinations, please refer to the Supplementary materials.

One significant limitation of the current demonstration is the low efficiency of single-photon detection, i.e. the camera, which results in significant noise and ex-

tended data acquisition times of eight minutes per polarization measurement. The camera's low efficiency of approximately 8% [35], combined with the need to couple polarization-entangled photons into single-mode fibers with a coupling efficiency of around 30%, only provides a coincidence efficiency of 0.06%. To improve the system's performance, a potential first step would be to generate entangled photons directly from fibers through spontaneous four-wave mixing [36], eliminating the losses associated with fiber coupling. This modification could result in an order of magnitude improvement in coincidence efficiency and, consequently, a reduction in data acquisition time. Moreover, with the coincidence efficiency scaling quadratically relative to the single-photon efficiency, further improvements could be achievable with the development of more sensitive cameras in the near future, allowing for entanglement characterization to be performed in mere seconds.

CONCLUSION AND OUTLOOK

In this study, we have successfully demonstrated the generation and characterization of non-uniform transverse polarization entanglement between various classes of vector beams in a scan-free manner. The demonstrated method can be invaluable for quickly characterizing spatially varying entanglement in EVBs, which are gaining interest in various high-dimensional quantum systems such as quantum communication and quantum imaging. We utilized spatial-temporal correlation measurements on data collected by a time-tagging event camera to perform polarization state tomography on approximately 2.6×10^6 (40×40) spatial modes using only 16 polarization measurements. The measurement results agreed well with theoretical predictions. Future improvements to the detection efficiency of time-tagging camera technology could potentially enable real-time state tomography on EVBs by splitting the beams onto multiple cameras, with each camera measuring a different polarization. These developments would significantly enhance the capabilities of quantum communication and quantum imaging systems. The local entanglement measurements in our system could be exploited to enhance the sensitivity of photonic gears [37, 38]. Our study also shows some promising applications, for example, quantum sensing of birefringent materials, and the generation of high-dimensional topological structures such as 4D-skyrmions.

[1] A. Einstein, B. Podolsky, and N. Rosen, *Can quantum-mechanical description of physical reality be considered complete?* *Phys. Rev.* **47**, 777 (1935).
 [2] Robert Raussendorf and Hans J. Briegel, *A one-way quantum computer*, *Phys. Rev. Lett.* **86**, 5188 (2001).

[3] Charles H. Bennett, Gilles Brassard, Claude Crépeau, Richard Jozsa, Asher Peres, and William K. Wootters, *Teleporting an unknown quantum state via dual classical and einstein-podolsky-rosen channels*, *Phys. Rev. Lett.* **70**, 1895 (1993).
 [4] Artur K. Ekert, *Quantum cryptography based on bell's theorem*, *Phys. Rev. Lett.* **67**, 661 (1991).
 [5] Charles H. Bennett and Stephen J. Wiesner, *Communication via one- and two-particle operators on einstein-podolsky-rosen states*, *Phys. Rev. Lett.* **69**, 2881 (1992).
 [6] Paul G. Kwiat, Aephraim M. Steinberg, and Raymond Y. Chiao, *Observation of a "quantum eraser": A revival of coherence in a two-photon interference experiment*, *Phys. Rev. A* **45**, 7729 (1992).
 [7] Ebrahim Karimi, Daniel Giovannini, Eliot Bolduc, Nicolas Bent, Filippo M. Miatto, Miles J. Padgett, and Robert W. Boyd, *Exploring the quantum nature of the radial degree of freedom of a photon via hong-ou-mandel interference*, *Phys. Rev. A* **89**, 013829 (2014).
 [8] Yingwen Zhang, Filippus S Roux, Thomas Konrad, Megan Agnew, Jonathan Leach, and Andrew Forbes, *Engineering two-photon high-dimensional states through quantum interference*, *Science advances* **2**, e1501165 (2016).
 [9] T. B. Pittman, D. V. Strelakov, A. Migdall, M. H. Rubin, A. V. Sergienko, and Y. H. Shih, *Can two-photon interference be considered the interference of two photons?* *Phys. Rev. Lett.* **77**, 1917 (1996).
 [10] J. Brendel, N. Gisin, W. Tittel, and H. Zbinden, *Pulsed energy-time entangled twin-photon source for quantum communication*, *Phys. Rev. Lett.* **82**, 2594 (1999).
 [11] Qiwen Zhan, *Cylindrical vector beams: from mathematical concepts to applications*, *Advances in Optics and Photonics* **1**, 1 (2009).
 [12] A. Bouhelier, M. Beversluis, A. Hartschuh, and L. Novotny, *Near-field second-harmonic generation induced by local field enhancement*, *Phys. Rev. Lett.* **90**, 013903 (2003).
 [13] Weibin Chen and Qiwen Zhan, *Numerical study of an apertureless near field scanning optical microscope probe under radial polarization illumination*, *Opt. Express* **15**, 4106 (2007).
 [14] Yuichi Kozawa and Shunichi Sato, *Optical trapping of micrometer-sized dielectric particles by cylindrical vector beams*, *Opt. Express* **18**, 10828 (2010).
 [15] Vincenzo D'ambrosio, Eleonora Nagali, Stephen P Walborn, Leandro Aolita, Sergei Slussarenko, Lorenzo Marrucci, and Fabio Sciarrino, *Complete experimental toolbox for alignment-free quantum communication*, *Nature communications* **3**, 1 (2012).
 [16] Osvaldo Jiménez Fariás, Vincenzo D'Ambrosio, Caterina Taballione, Fabrizio Bisesto, Sergei Slussarenko, Leandro Aolita, Lorenzo Marrucci, Stephen P Walborn, and Fabio Sciarrino, *Resilience of hybrid optical angular momentum qubits to turbulence*, *Scientific reports* **5**, 1 (2015).
 [17] Bienvenu Ndagano, Isaac Nape, Mitchell A Cox, Carmelo Rosales-Guzman, and Andrew Forbes, *Creation and detection of vector vortex modes for classical and quantum communication*, *Journal of Lightwave Technology* **36**, 292 (2018).
 [18] R. Dorn, S. Quabis, and G. Leuchs, *Sharper focus for a radially polarized light beam*, *Phys. Rev. Lett.* **91**, 233901 (2003).

- [19] Haifeng Wang, Luping Shi, Boris Lukyanchuk, Colin Sheppard, and Chong Tow Chong, *Creation of a needle of longitudinally polarized light in vacuum using binary optics*, *Nature photonics* **2**, 501 (2008).
- [20] CER Souza, CVS Borges, AZ Khoury, JAO Huguénin, L Aolita, and SP Walborn, *Quantum key distribution without a shared reference frame*, *Physical Review A* **77**, 032345 (2008).
- [21] Giuseppe Vallone, Vincenzo D’Ambrosio, Anna Sponelli, Sergei Slussarenko, Lorenzo Marrucci, Fabio Sciarrino, and Paolo Villoresi, *Free-space quantum key distribution by rotation-invariant twisted photons*, *Phys. Rev. Lett.* **113**, 060503 (2014).
- [22] Kyosuke Sakai and S Noda, *Optical trapping of metal particles in doughnut-shaped beam emitted by photonic-crystal laser*, *Electronics Letters* **43**, 1 (2007).
- [23] Eiji Miyai, Kyosuke Sakai, Takayuki Okano, Wataru Kunishi, Dai Ohnishi, and Susumu Noda, *Lasers producing tailored beams*, *Nature* **441**, 946 (2006).
- [24] Seita Iwahashi, Yoshitaka Kurosaka, Kyosuke Sakai, Kyoko Kitamura, Naoki Takayama, and Susumu Noda, *Higher-order vector beams produced by photonic-crystal lasers*, *Opt. Express* **19**, 11963 (2011).
- [25] Filippo Cardano, Ebrahim Karimi, Sergei Slussarenko, Lorenzo Marrucci, Corrado de Lisio, and Enrico Santamato, *Polarization pattern of vector vortex beams generated by q-plates with different topological charges*, *Appl. Opt.* **51**, C1 (2012).
- [26] Filippo Cardano, Ebrahim Karimi, Lorenzo Marrucci, Corrado de Lisio, and Enrico Santamato, *Generation and dynamics of optical beams with polarization singularities*, *Opt. Express* **21**, 8815 (2013).
- [27] Robert Fickler, Mario Krenn, Radek Lapkiewicz, Sven Ramelow, and Anton Zeilinger, *Real-time imaging of quantum entanglement*, *Scientific reports* **3**, 1 (2013).
- [28] Vincenzo D’Ambrosio, Gonzalo Carvacho, Francesco Graffitti, Chiara Vitelli, Bruno Piccirillo, Lorenzo Marrucci, and Fabio Sciarrino, *Entangled vector vortex beams*, *Phys. Rev. A* **94**, 030304 (2016).
- [29] Francesco Graffitti, Vincenzo D’Ambrosio, Massimiliano Proietti, Joseph Ho, Bruno Piccirillo, Corrado de Lisio, Lorenzo Marrucci, and Alessandro Fedrizzi, *Hyperentanglement in structured quantum light*, *Phys. Rev. Research* **2**, 043350 (2020).
- [30] J.B. Altepeter, E.R. Jeffrey, and P.G. Kwiat, *Photonic state tomography*, *Advances In Atomic, Molecular, and Optical Physics*, **52**, 105 (2005).
- [31] Robert Fickler, Radek Lapkiewicz, Sven Ramelow, and Anton Zeilinger, *Quantum entanglement of complex photon polarization patterns in vector beams*, *Phys. Rev. A* **89**, 060301 (2014).
- [32] Ebrahim Karimi, Bruno Piccirillo, Lorenzo Marrucci, and Enrico Santamato, *Light propagation in a birefringent plate with topological charge*, *Optics letters* **34**, 1225 (2009).
- [33] Ebrahim Karimi, Gianluigi Zito, Bruno Piccirillo, Lorenzo Marrucci, and Enrico Santamato, *Hypergeometric-gaussian modes*, *Optics letters* **32**, 3053 (2007).
- [34] Sergei Slussarenko, Anatoli Murauski, Tao Du, Vladimir Chigrinov, Lorenzo Marrucci, and Enrico Santamato, *Tunable liquid crystal q-plates with arbitrary topological charge*, *Optics express* **19**, 4085 (2011).
- [35] Victor Vidyapin, Yingwen Zhang, Duncan England, and Benjamin Sussman, *Characterisation of a single photon event camera for quantum imaging*, (2022).
- [36] Hiroki Takesue and Kyo Inoue, *Generation of polarization-entangled photon pairs and violation of bell’s inequality using spontaneous four-wave mixing in a fiber loop*, *Phys. Rev. A* **70**, 031802 (2004).
- [37] Vincenzo D’ambrosio, Nicolo Spagnolo, Lorenzo Del Re, Sergei Slussarenko, Ying Li, Leong Chuan Kwek, Lorenzo Marrucci, Stephen P Walborn, Leandro Aolita, and Fabio Sciarrino, *Photonic polarization gears for ultra-sensitive angular measurements*, *Nature communications* **4**, 2432 (2013).
- [38] Raouf Barboza, Amin Babazadeh, Lorenzo Marrucci, Filippo Cardano, Corrado de Lisio, and Vincenzo D’Ambrosio, *Ultra-sensitive measurement of transverse displacements with linear photonic gears*, *Nature Communications* **13**, 1080 (2022).
- [39] <https://www.amscins.com/tpx3cam/>, .
- [40] Andrei Nomerotski, *Imaging and time stamping of photons with nanosecond resolution in timepix based optical cameras*, *Nuclear Instruments and Methods in Physics Research Section A: Accelerators, Spectrometers, Detectors and Associated Equipment* **937**, 26 (2019).

Acknowledgments The authors would like to thank Ryan Hogan for helping with coding during the data analysis, and Paul Corkum, Felix Hufnagel, Dilip Paneru, and Frédéric Bouchard for their valuable discussions. K.H. acknowledges that the National Research Council of Canada (NRC) headquarters is located on the traditional unceded territory of the Algonquin Anishinaabe and Mohawk people. This work was supported by the Canada Research Chairs (CRC), the High Throughput and Secure Networks (HTSN) Challenge Program at the National Research Council of Canada, and the Joint Centre for Extreme Photonics (JCEP).

Author Contributions E.K. conceived the idea. X.G. and Y.Z. devised the experimental setup. X.G. performed the experiment. A.S. and A.D. fabricated q-plates. X.G., Y.Z., and A.D. analyzed the data. K.H., P.C. and E.K. supervised the project. All authors contributed to the writing of the manuscript.

Data availability The data that support the findings of this study are available from the corresponding author upon reasonable request.

Code availability The code used for the data analysis is available from the corresponding author upon reasonable request.

Ethics declarations The authors declare no competing interests.

Corresponding authors Correspondence and requests for materials should be addressed to yzhang6@uottawa.ca.

METHODS

The experimental setup for generation and characterization of entangled vector beams is shown in Fig. 4. The setup can be divided into three stages: EPR Pair Generation, State Preparation, and State Tomography. In the EPR Pair Generation stage, a 5-mm-thick Type-II periodically poled potassium titanyl phosphate (ppKTP) crystal is pumped by a 405 nm continuous-wave laser to generate photon pairs with orthogonal polarization through the process of spontaneous parametric down-conversion (SPDC). The photon pairs then go through two-photon interference in a Hong-Ou-Mandel interferometer which will act as a filter for the antisymmetric $|\psi^-\rangle$ Bell state,

$$|\Psi_0\rangle = \frac{1}{\sqrt{2}}(|H\rangle_s |V\rangle_i - |V\rangle_s |H\rangle_i), \quad (6)$$

when time correlation measurements between the two exit ports of the interferometer are made. Performing polarization state tomography at this stage between the two exit ports precisely gives the $|\psi^-\rangle$ Bell state where the reconstructed density matrix can be seen in the inset of Fig. 4 with a concurrence and purity of $\sim 99\%$. In the State Preparation stage, the polarization entangled photon pair is first coupled into single-mode fibers (SMFs) for spatial mode filtering leaving only the Gaussian mode on exit while still maintaining polarization entanglement. q -plates are then used to transform the spatially uniform polarization entanglement into entangled vector beams with spatially varying polarization entanglement. Lastly, in the State Tomography stage, polarization state tomography is performed through 16 different polarization measurements using a series of a quarter-wave plate, half-wave plate, and polarizing beamsplitter after which each photon of the entangled pair is guided to hit a different region of a time-tagging event camera (TPX3CAM [39, 40]) where spatial and temporal information of the photons are recorded from which spatial-temporal correlation measurements are made.

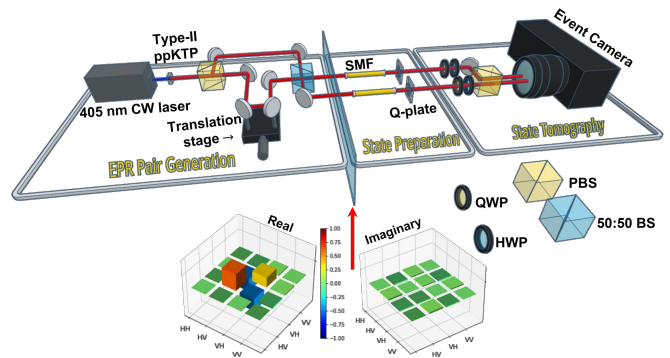


FIG. 4. **Experimental setup for generation and characterization of entangled vector beams.** EPR Pair Generation - A Type-II ppKTP crystal is pumped by a 405 nm continuous-wave laser to generate photon pairs orthogonal in polarization through SPDC. An antisymmetric Bell state $|\psi^-\rangle$ is generated through correlation measurements between the two exit ports of a Hong-Ou-Mandel interferometer. State Preparation - The polarization-entangled photon pair are first coupled into single-mode fibers (SMFs) for spatial mode filtering. q -plates are then used to transform the spatially uniform polarization entanglement into entangled vector beams. State Tomography - Polarization state tomography is performed using a series of a quarter-wave plate (QWP), a half-wave plate (HWP), and a Polarizing beamsplitter (PBS) after which each photon of the entangled pair is guided to hit a different region of an event camera where spatial and temporal information of the photons are recorded. The inset below the experimental setup shows the polarization density matrix (real and imaginary) measured after the EPR Pair Generation stage with the entanglement being in the $|\psi^-\rangle$ Bell state.

Supplementary Materials for: Full spatial characterization of entangled structured photons

TWO TUNED q -PLATES

The unitary action \hat{U}_q^δ of a q -plate with topological charge q acting on a circularly polarized Gaussian beam to first-order approximation can be written as

$$\hat{U}_q^\delta \cdot \begin{bmatrix} |L\rangle \\ |R\rangle \end{bmatrix} = F_0(r) \cos(\delta/2) \begin{bmatrix} |L\rangle \\ |R\rangle \end{bmatrix} + i \sin(\delta/2) F_q(r) \begin{bmatrix} e^{-i2q\theta} |R\rangle \\ e^{i2q\theta} |L\rangle \end{bmatrix}, \quad (\text{S1})$$

where $|L\rangle$ and $|R\rangle$ are left- and right-circular polarizations respectively. $F_q(r)e^{\pm i2q\theta} \equiv \text{LG}_{0,\pm 2q}(r, \theta)$ is the Laguerre-Gauss mode with orbital angular momentum index $2q$ and radial index zero at $z = 0$. $\delta \in [0, \pi]$ is an adjustable parameter that can be tuned based on the voltage applied to the q -plate. The q -plates are considered tuned with $\delta = \pi$, and when $\delta = \pi/2$, the q -plates are considered partially tuned.

In our work, we first prepare an anti-symmetric entangled state in the polarization degree of freedom (DOF),

$$\begin{aligned} |\Psi_0\rangle &= \frac{1}{\sqrt{2}}(|H\rangle_s |V\rangle_i - |V\rangle_s |H\rangle_i) \\ &= \frac{i}{\sqrt{2}}(|L\rangle_s |R\rangle_i - |R\rangle_s |L\rangle_i), \end{aligned} \quad (\text{S2})$$

with s and i denoting the signal and idler photons respectively.

Applying two tuned q -plates ($\delta_s = \delta_i = \pi$) with topological charges q_s and q_i respectively to each photon gives the following final state,

$$|\Psi_f\rangle = \frac{i}{\sqrt{2}} F_{q_s, q_i}(r_s, r_i) \left[e^{-2i(q_s\theta_s - q_i\theta_i)} |R\rangle_s |L\rangle_i - e^{2i(q_s\theta_s - q_i\theta_i)} |L\rangle_s |R\rangle_i \right], \quad (\text{S3})$$

where $F_{q_s, q_i}(r_s, r_i) = F_{q_s}(r_s)F_{q_i}(r_i)$.

Rewriting in the horizontal (H) and vertical (V) polarization basis gives

$$|\Psi_f\rangle = F_{q_s, q_i}(r_s, r_i) \left[\sin 2(q_s\theta_s - q_i\theta_i) |\phi^+\rangle - \cos 2(q_s\theta_s - q_i\theta_i) |\psi^-\rangle \right]. \quad (\text{S4})$$

where $|\phi^+\rangle = \frac{1}{\sqrt{2}}(|H\rangle_s |H\rangle_i + |V\rangle_s |V\rangle_i)$ and $|\psi^-\rangle = \frac{1}{\sqrt{2}}(|H\rangle_s |V\rangle_i - |V\rangle_s |H\rangle_i)$ are two of the four Bell states.

Therefore, the probabilities for the final state to be in one of the four Bell states are as follows,

$$\begin{aligned} P_{\phi^+}^t &= F_{q_s, q_i}^2(r_s, r_i) \sin^2 2(q_s\theta_s - q_i\theta_i) \\ P_{\phi^-}^t &= 0 \\ P_{\psi^+}^t &= 0 \\ P_{\psi^-}^t &= F_{q_s, q_i}^2(r_s, r_i) \cos^2 2(q_s\theta_s - q_i\theta_i) \end{aligned} \quad (\text{S5})$$

TWO PARTIALLY TUNED q -PLATES

When using two partially tuned q -plates ($\delta = \pi/2$), the initial entangled state from Eq.(S2) becomes,

$$\begin{aligned} |\Psi_f\rangle &= \frac{i}{2\sqrt{2}} \left\{ (F_{0,0}(r_s, r_i) - F_{q_s, q_i}(r_s, r_i) e^{2i(q_s\theta_s - q_i\theta_i)} |L\rangle_s |R\rangle_i \right. \\ &\quad - [F_{0,0}(r_s, r_i) - F_{q_s, q_i}(r_s, r_i) e^{-2i(q_s\theta_s - q_i\theta_i)}] |R\rangle_s |L\rangle_i \\ &\quad + [F_{0, q_i}(r_s, r_i)(r_i) e^{2iq_i\theta_i} - F_{q_s, 0}(r_s, r_i) e^{2iq_s\theta_s}] |L\rangle_s |L\rangle_i \\ &\quad \left. - [F_{0, q_i}(r_s, r_i)(r_i) e^{-2iq_i\theta_i} - F_{q_s, 0}(r_s, r_i) e^{-2iq_s\theta_s}] |R\rangle_s |R\rangle_i \right\}. \end{aligned} \quad (\text{S6})$$

Rewriting in the H and V basis gives

$$\begin{aligned}
|\Psi_f\rangle = & \frac{1}{2} \left\{ -F_{q_s, q_i}(r_s, r_i) \sin 2(q_s \theta_s - q_i \theta_i) |\phi^+\rangle \right. \\
& + [F_{0,0}(r_s, r_i) - F_{q_s, q_i}(r_s, r_i) \sin 2(q_s \theta_s - q_i \theta_i)] |\psi^-\rangle \\
& + [F_{0, q_i}(r_s, r_i) \sin 2q_i \theta_i - F_{q_s, 0}(r_s, r_i) \sin 2q_s \theta_s] |\phi^-\rangle \\
& \left. + [F_{0, q_i}(r_s, r_i) \cos 2q_i \theta_i - F_{q_s, 0}(r_s, r_i) \cos 2q_s \theta_s] |\psi^+\rangle \right\}, \tag{S7}
\end{aligned}$$

with $|\phi^\pm\rangle = \frac{1}{\sqrt{2}}(|H\rangle_s |H\rangle_i \pm |V\rangle_s |V\rangle_i)$, and $|\psi^\pm\rangle = \frac{1}{\sqrt{2}}(|H\rangle_s |V\rangle_i \pm |V\rangle_s |H\rangle_i)$ being the four Bell states.

Thus, the probabilities for the final state to be in one of the four Bell states are as follows,

$$\begin{aligned}
P_{\phi^+}^{\text{pt}} &= \frac{1}{4} F_{q_s, q_i}^2(r_s, r_i) \sin^2 2(q_s \theta_s - q_i \theta_i) \\
P_{\phi^-}^{\text{pt}} &= \frac{1}{4} [F_{0, q_i}(r_s, r_i) \sin 2q_i \theta_i - F_{q_s, 0}(r_s, r_i) \sin 2q_s \theta_s]^2 \\
P_{\psi^+}^{\text{pt}} &= \frac{1}{4} [F_{0, q_i}(r_s, r_i) \cos 2q_i \theta_i - F_{q_s, 0}(r_s, r_i) \cos 2q_s \theta_s]^2 \\
P_{\psi^-}^{\text{pt}} &= \frac{1}{4} [F_{0, 0}(r_s, r_i) - F_{q_s, q_i}(r_s, r_i) \sin 2(q_s \theta_s - q_i \theta_i)]^2. \tag{S8}
\end{aligned}$$

EXPERIMENTAL RESULTS

To verify and characterize the entanglement with vector beams, we measured the correlations in the radial and angular coordinates between two structured beams and observed the generated state changes angularly among the four Bell states, as shown in Figs. [S1](#) - [S12](#).

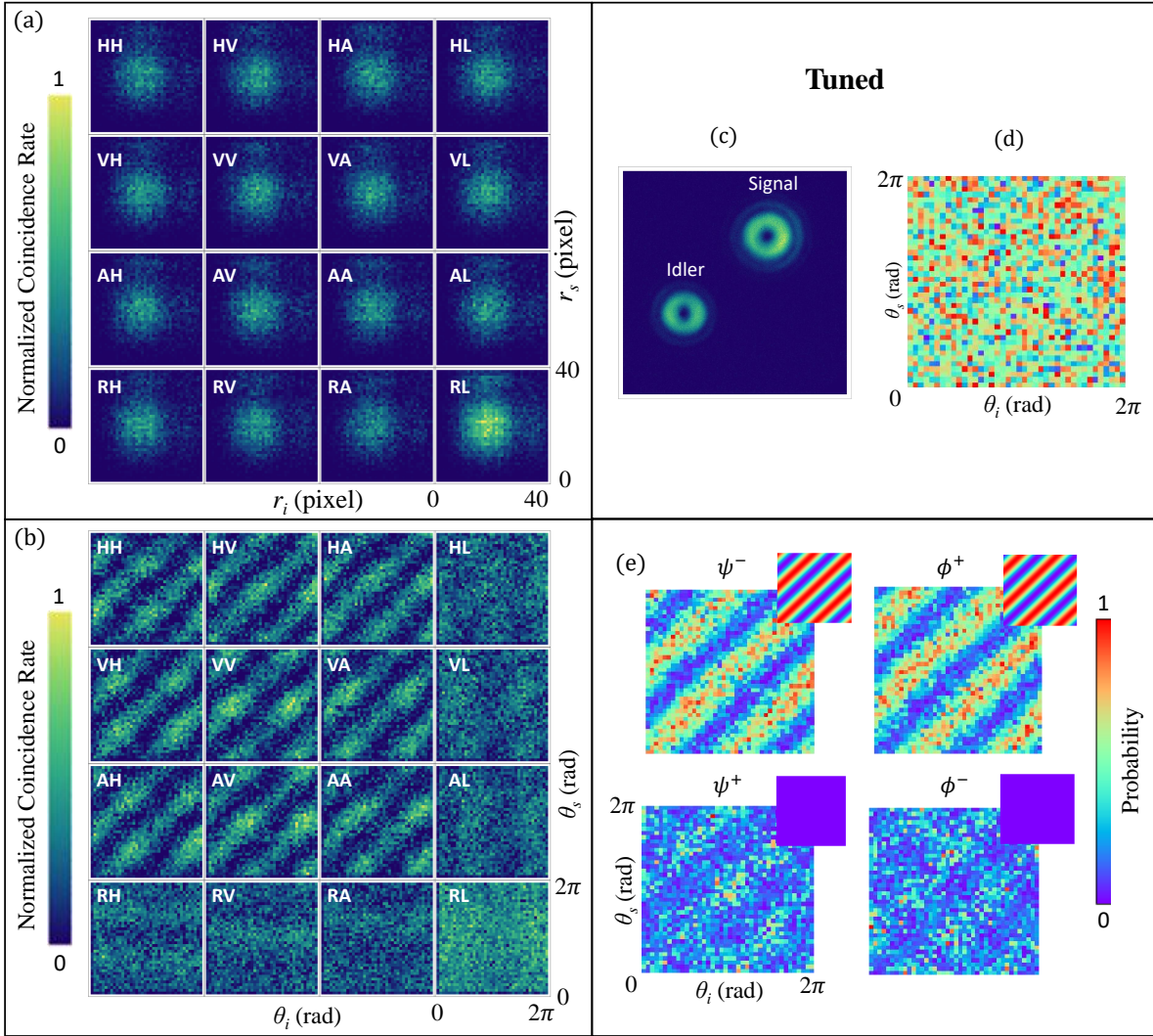


Figure S1. Measured spatial correlations and entanglement characterization for bi-photon with spatially varying polarization states generated via two q -plates. (a)-(b) Two-photon spatial correlations between two entangled vector beams measured, in the radial and azimuthal DOF respectively, from 16 different polarization measurements. Two tuned q -plates ($\delta_s = \delta_i = \pi$) with topological charges $q_i = 1/2$ and $q_s = 1/2$ are used to generate the entangled vector vortex photons. (c) Continuous exposure images recorded on the camera. (d) The concurrence of the entangled state and the average concurrence is measured to be 0.566 ± 0.035 . (e) Reconstructed probabilities for the four Bell states $\{|\psi^+\rangle, |\psi^-\rangle, |\phi^+\rangle, |\phi^-\rangle\}$. The insets are the respective theoretical probabilities.

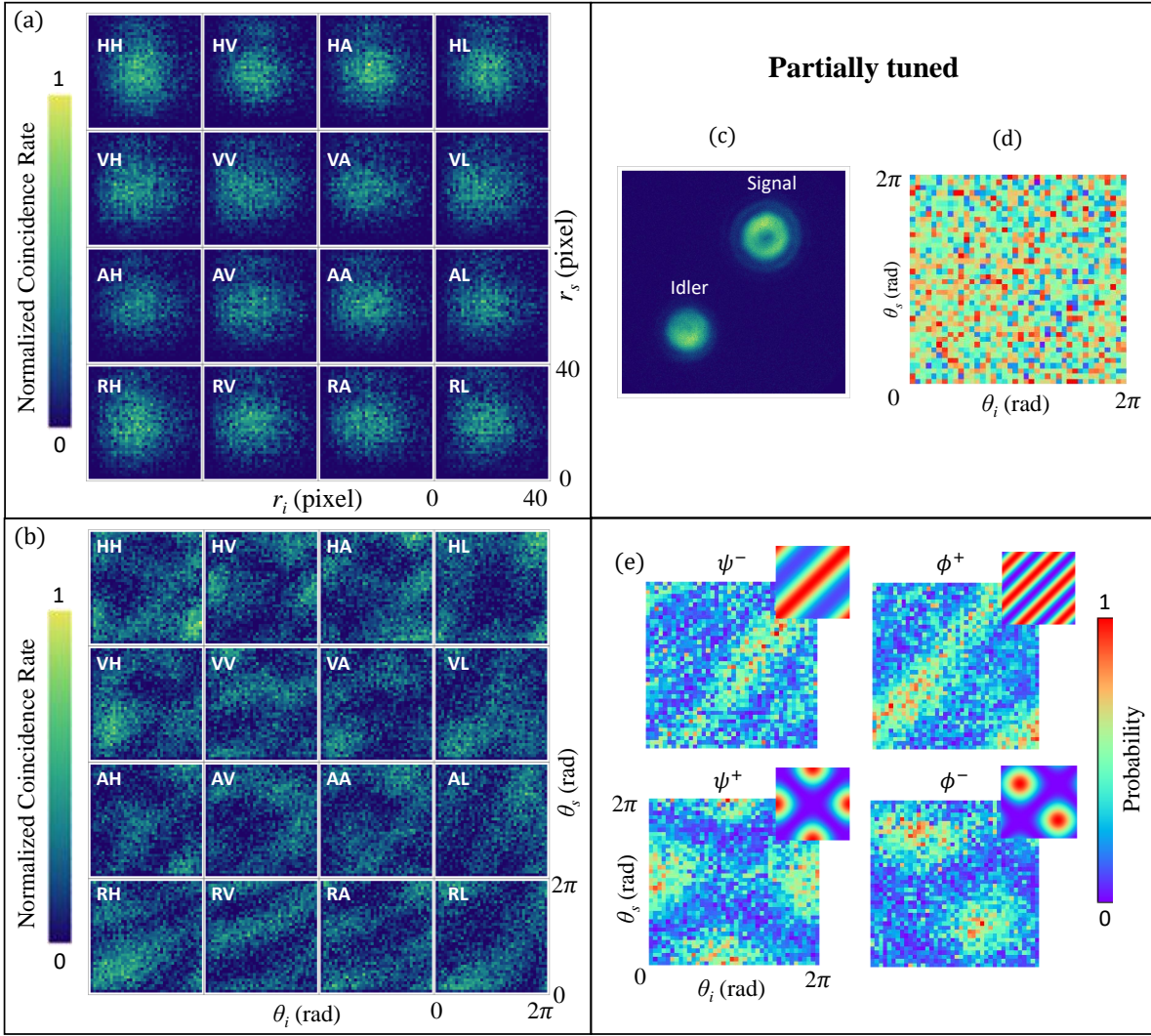


Figure S2. Measured spatial correlations and entanglement characterization for bi-photon with spatially varying polarization states generated via two q -plates. (a)-(b) Two-photon spatial correlations between two entangled vector beams measured, in the radial and azimuthal DOF respectively, from 16 different polarization measurements. Two partially tuned q -plates ($\delta_s = \delta_i = \pi/2$) with topological charges $q_i = 1/2$ and $q_s = 1/2$ are used to generate the entangled vector vortex photons. (c) Continuous exposure images recorded on the camera. (d) The concurrence of the entangled state and the average concurrence is measured to be 0.556 ± 0.079 . (e) Reconstructed probabilities for the four Bell states $\{|\psi^+\rangle, |\psi^-\rangle, |\phi^+\rangle, |\phi^-\rangle\}$. The insets are the respective theoretical probabilities.

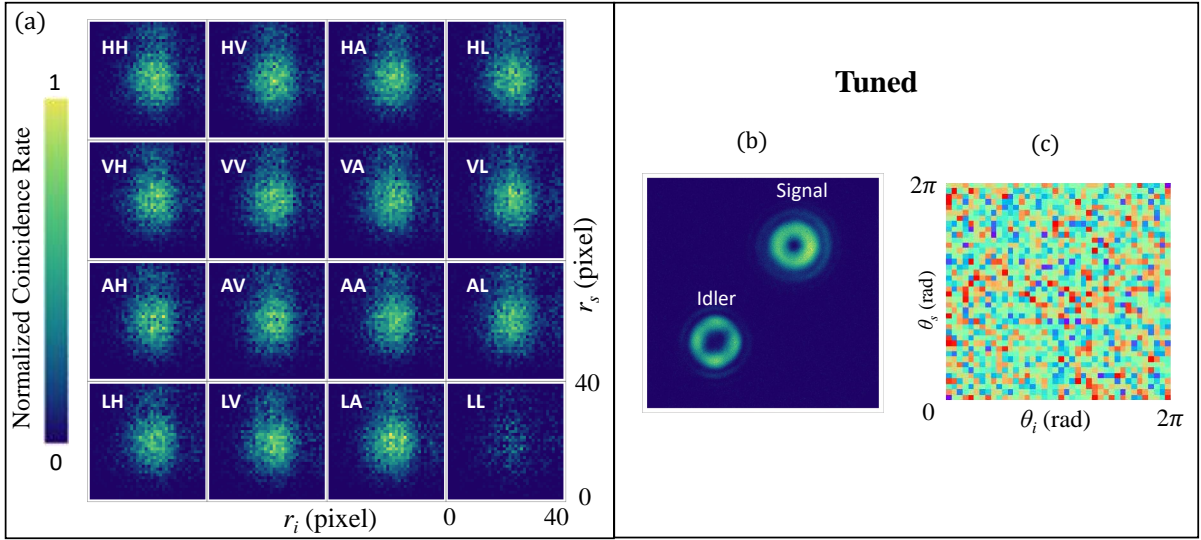


Figure S3. Measured spatial correlations and entanglement characterization for bi-photon with spatially varying polarization states generated via two q -plates. (a) Two-photon spatial correlations between two entangled vector beams measured, in the radial coordinate respectively, from 16 different polarization measurements. Two tuned q -plates ($\delta_s = \delta_i = \pi$) with topological charges $q_i = 1$ and $q_s = 1/2$ are used to generate the entangled vector vortex photons. (b) Continuous exposure images recorded on the camera. (c) The concurrence of the entangled state and the average concurrence is measured to be 0.540 ± 0.005 .

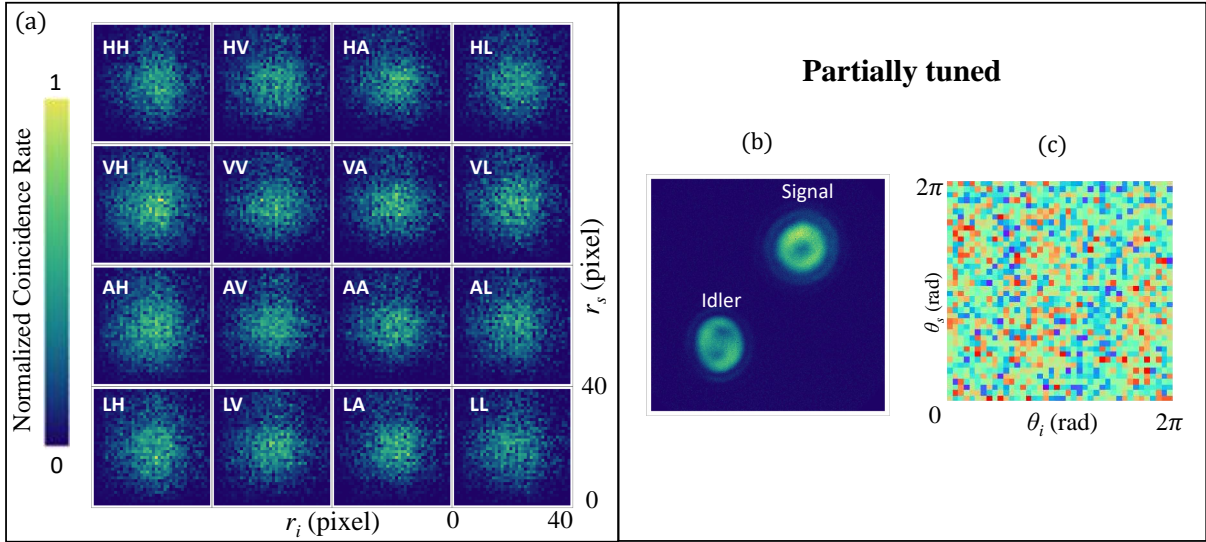


Figure S4. Measured spatial correlations and entanglement characterization for bi-photon with spatially varying polarization states generated via two q -plates. (a) Two-photon spatial correlations between two entangled vector beams measured, in the radial coordinate respectively, from 16 different polarization measurements. Two partially tuned q -plates ($\delta_s = \delta_i = \pi/2$) with topological charges $q_i = 1$ and $q_s = 1/2$ are used to generate the entangled vector vortex photons. (b) Continuous exposure images recorded on the camera. (c) The concurrence of the entangled state and the average concurrence is measured to be 0.517 ± 0.005 .

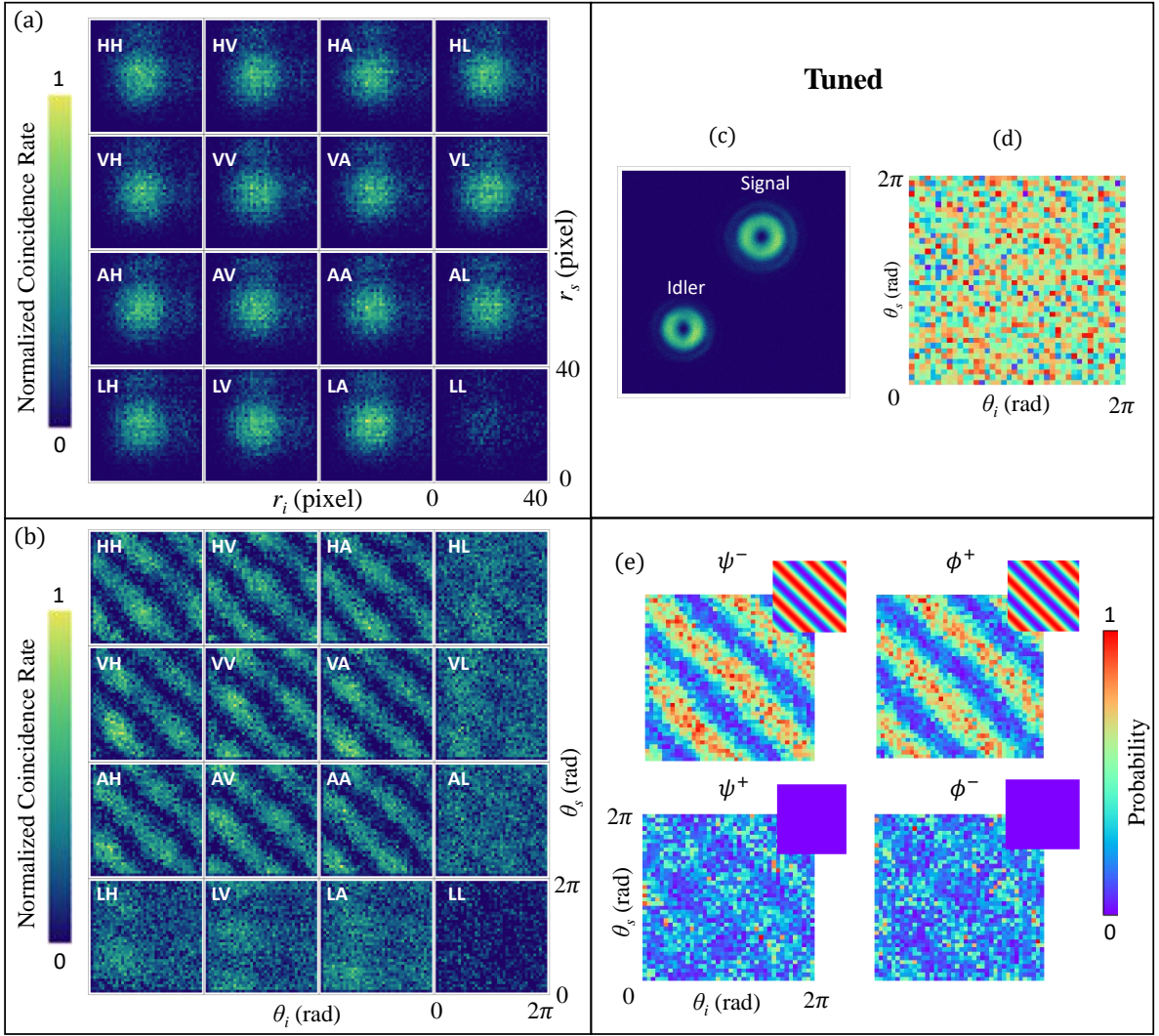


Figure S5. Measured spatial correlations and entanglement characterization for bi-photon with spatially varying polarization states generated via two q -plates. (a)-(b) Two-photon spatial correlations between two entangled vector beams measured, in the radial and azimuthal DOF respectively, from 16 different polarization measurements. Two tuned q -plates ($\delta_s = \delta_i = \pi$) with topological charges $q_i = -1/2$ and $q_s = 1/2$ are used to generate the entangled vector vortex photons. (c) Continuous exposure images recorded on the camera. (d) The concurrence of the entangled state and the average concurrence is measured to be 0.575 ± 0.010 . (e) Reconstructed probabilities for the four Bell states $\{|\psi^+\rangle, |\psi^-\rangle, |\phi^+\rangle, |\phi^-\rangle\}$. The insets are the respective theoretical probabilities.

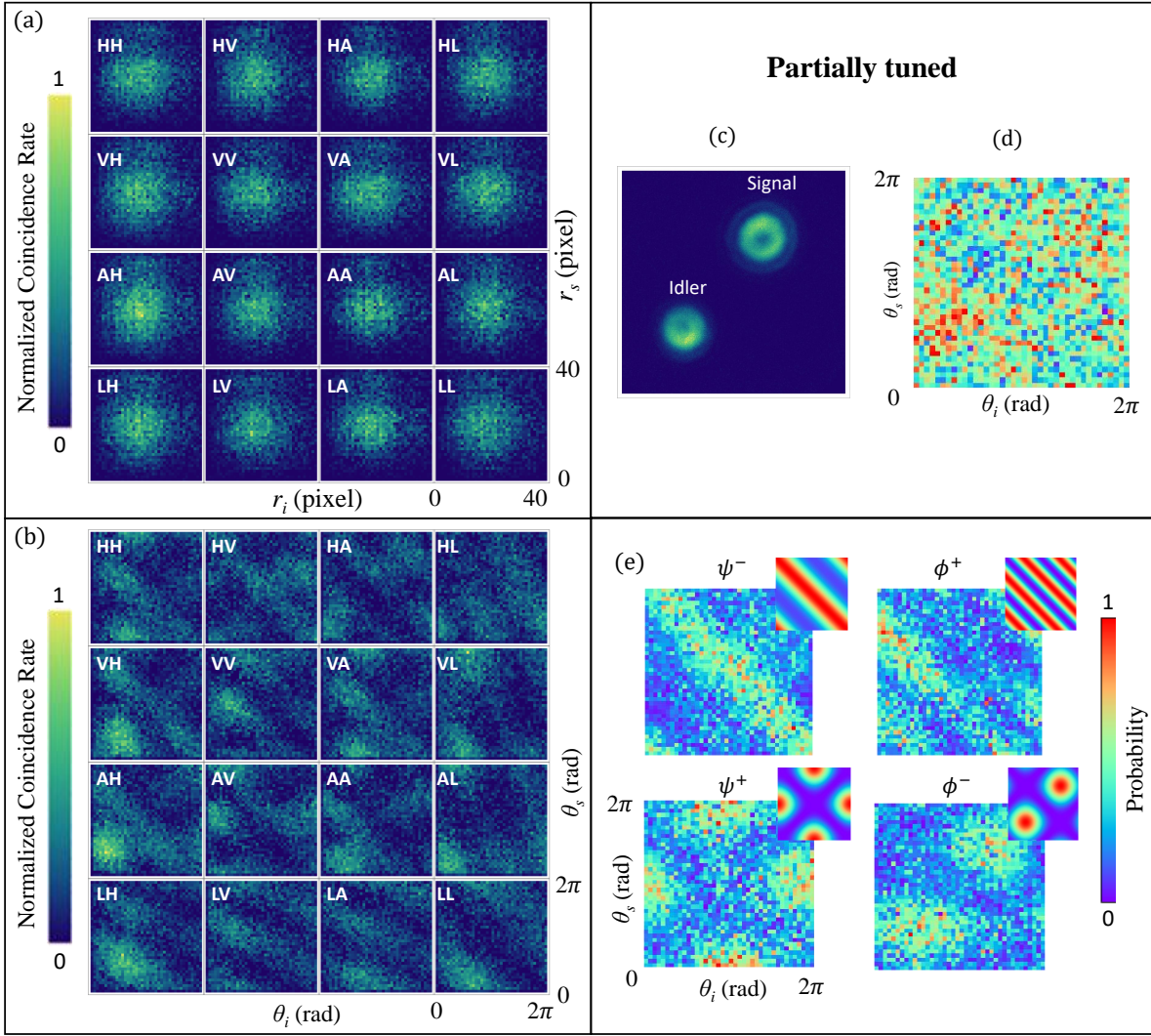


Figure S6. Measured spatial correlations and entanglement characterization for bi-photon with spatially varying polarization states generated via two q -plates. (a)-(b) Two-photon spatial correlations between two entangled vector beams measured, in the radial and azimuthal DOF respectively, from 16 different polarization measurements. Two partially tuned q -plates ($\delta_s = \delta_i = \pi/2$) with topological charges $q_i = -1/2$ and $q_s = 1/2$ are used to generate the entangled vector vortex photons. (c) Continuous exposure images recorded on the camera. (d) The concurrence of the entangled state and the average concurrence is measured to be 0.519 ± 0.006 . (e) Reconstructed probabilities for the four Bell states $\{|\psi^+\rangle, |\psi^-\rangle, |\phi^+\rangle, |\phi^-\rangle\}$. The insets are the respective theoretical probabilities.

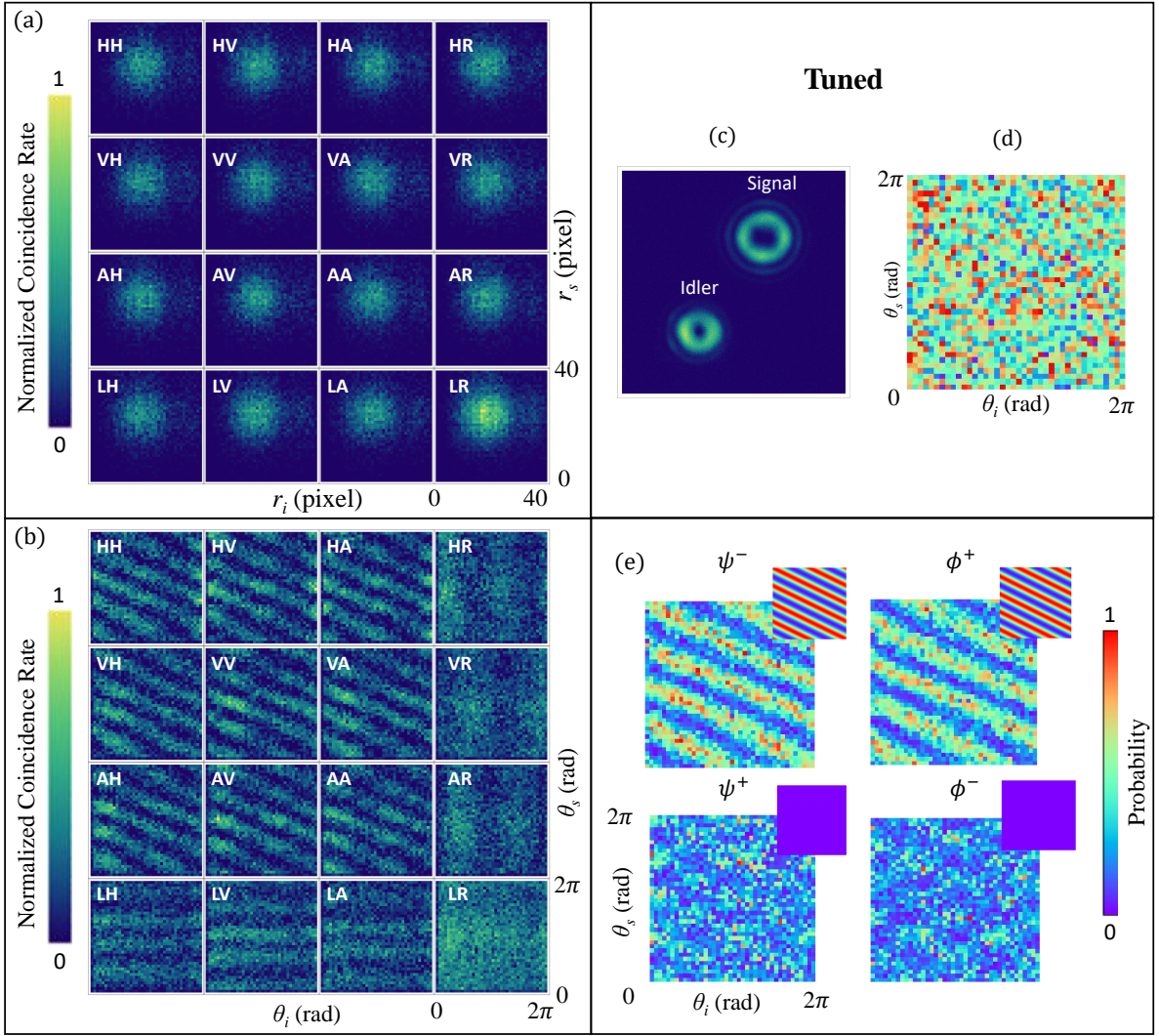


Figure S7. Measured spatial correlations and entanglement characterization for bi-photon with spatially varying polarization states generated via two q -plates. (a)-(b) Two-photon spatial correlations between two entangled vector beams measured, in the radial and azimuthal DOF respectively, from 16 different polarization measurements. Two tuned q -plates ($\delta_s = \delta_i = \pi$) with topological charges $q_i = -1/2$ and $q_s = 1$ are used to generate the entangled vector vortex photons. (c) Continuous exposure images recorded on the camera. (d) The concurrence of the entangled state and the average concurrence is measured to be 0.548 ± 0.018 . (e) Reconstructed probabilities for the four Bell states $\{|\psi^+\rangle, |\psi^-\rangle, |\phi^+\rangle, |\phi^-\rangle\}$. The insets are the respective theoretical probabilities.

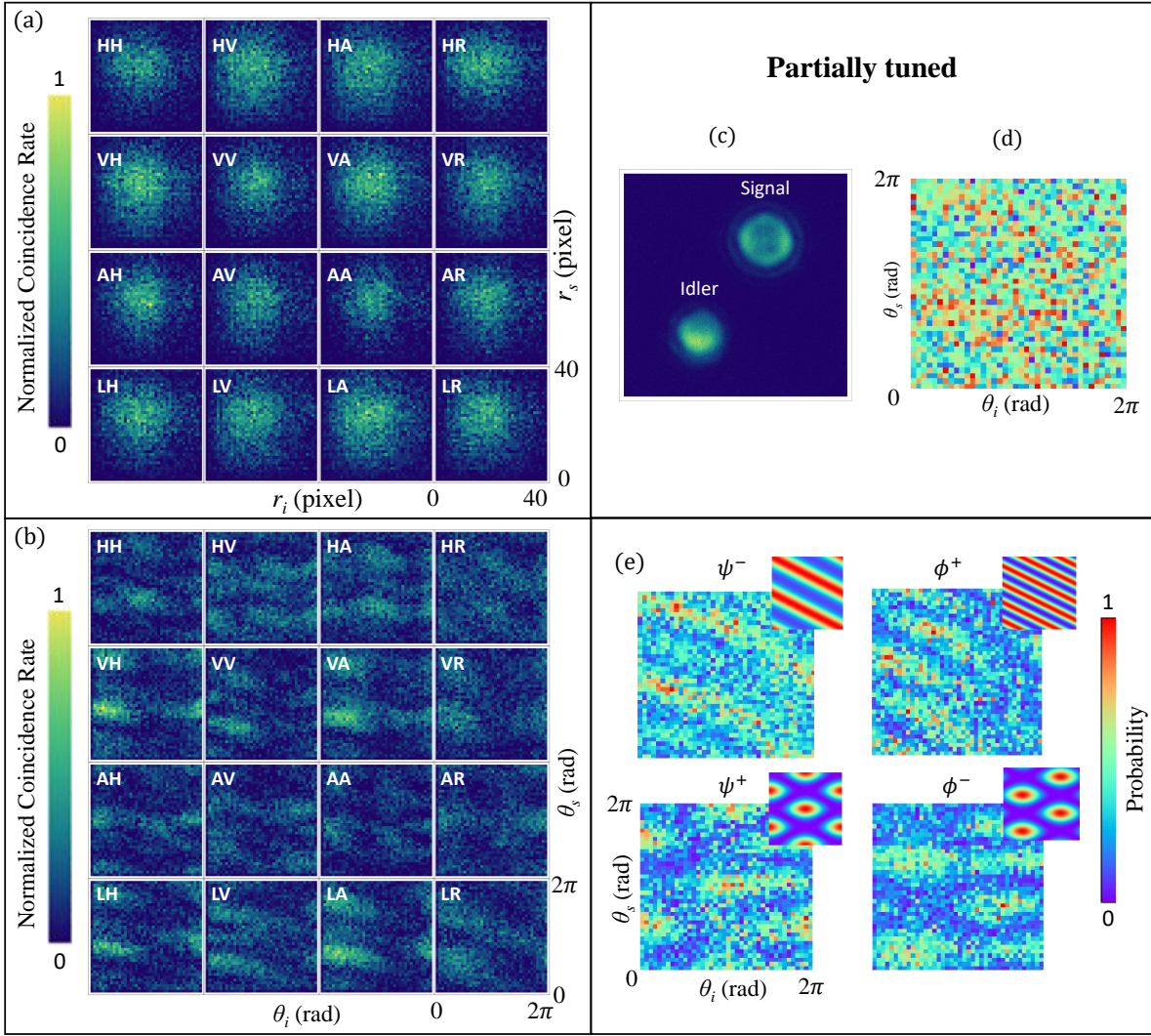


Figure S8. Measured spatial correlations and entanglement characterization for bi-photon with spatially varying polarization states generated via two q -plates. (a)-(b) Two-photon spatial correlations between two entangled vector beams measured, in the radial and azimuthal DOF respectively, from 16 different polarization measurements. Two partially tuned q -plates ($\delta_s = \delta_i = \pi/2$) with topological charges $q_i = -1/2$ and $q_s = 1$ are used to generate the entangled vector vortex photons. (c) Continuous exposure images recorded on the camera. (d) The concurrence of the entangled state and the average concurrence is measured to be 0.525 ± 0.010 . (e) Reconstructed probabilities for the four Bell states $\{|\psi^+\rangle, |\psi^-\rangle, |\phi^+\rangle, |\phi^-\rangle\}$. The insets are the respective theoretical probabilities.

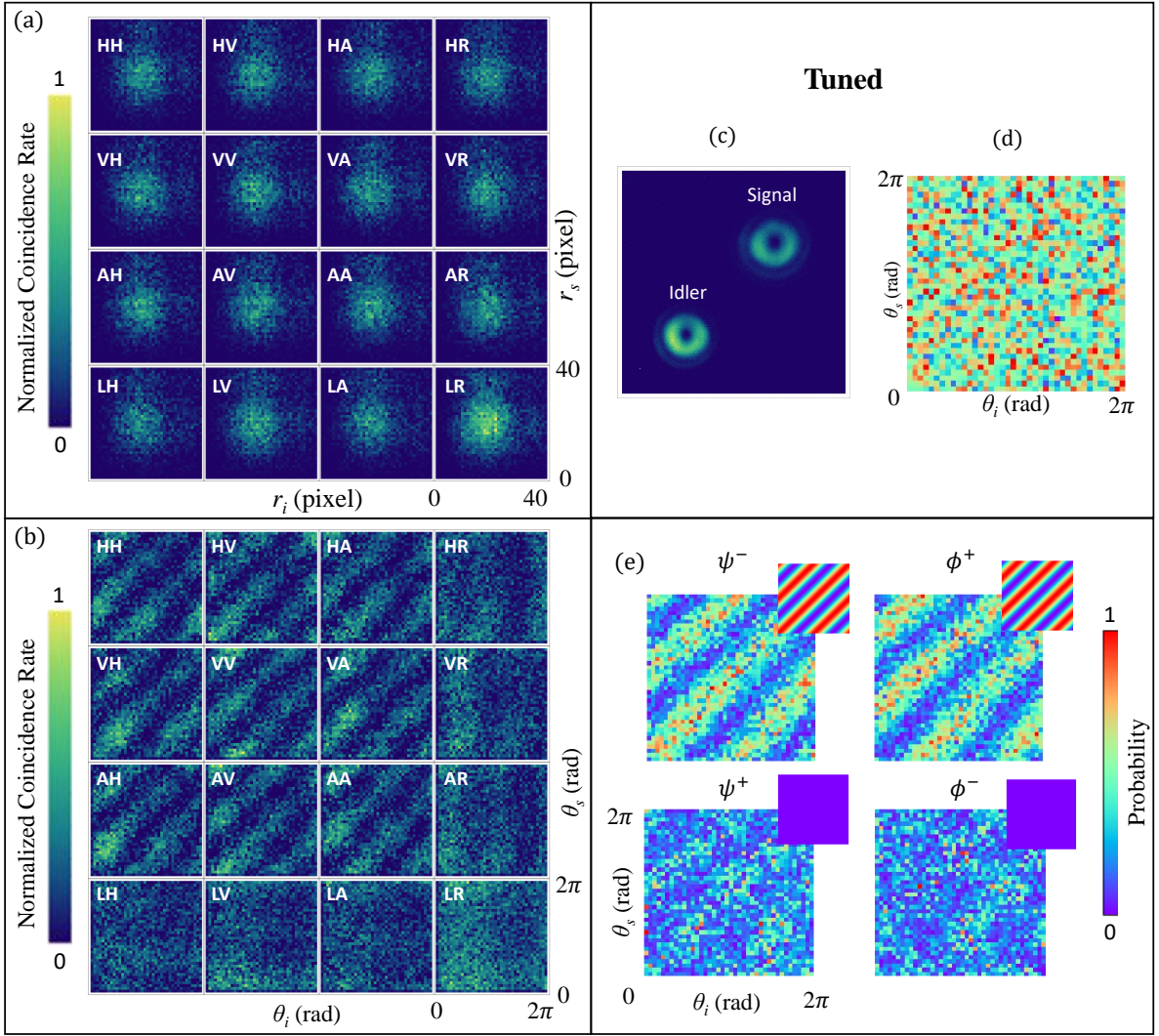


Figure S9. Measured spatial correlations and entanglement characterization for bi-photon with spatially varying polarization states generated via two q -plates. (a)-(b) Two-photon spatial correlations between two entangled vector beams measured, in the radial and azimuthal DOF respectively, from 16 different polarization measurements. Two tuned q -plates ($\delta_s = \delta_i = \pi$) with topological charges $q_i = -1/2$ and $q_s = -1/2$ are used to generate the entangled vector vortex photons. (c) Continuous exposure images recorded on the camera. (d) The concurrence of the entangled state and the average concurrence is measured to be 0.555 ± 0.005 . (e) Reconstructed probabilities for the four Bell states $\{|\psi^+\rangle, |\psi^-\rangle, |\phi^+\rangle, |\phi^-\rangle\}$. The insets are the respective theoretical probabilities.

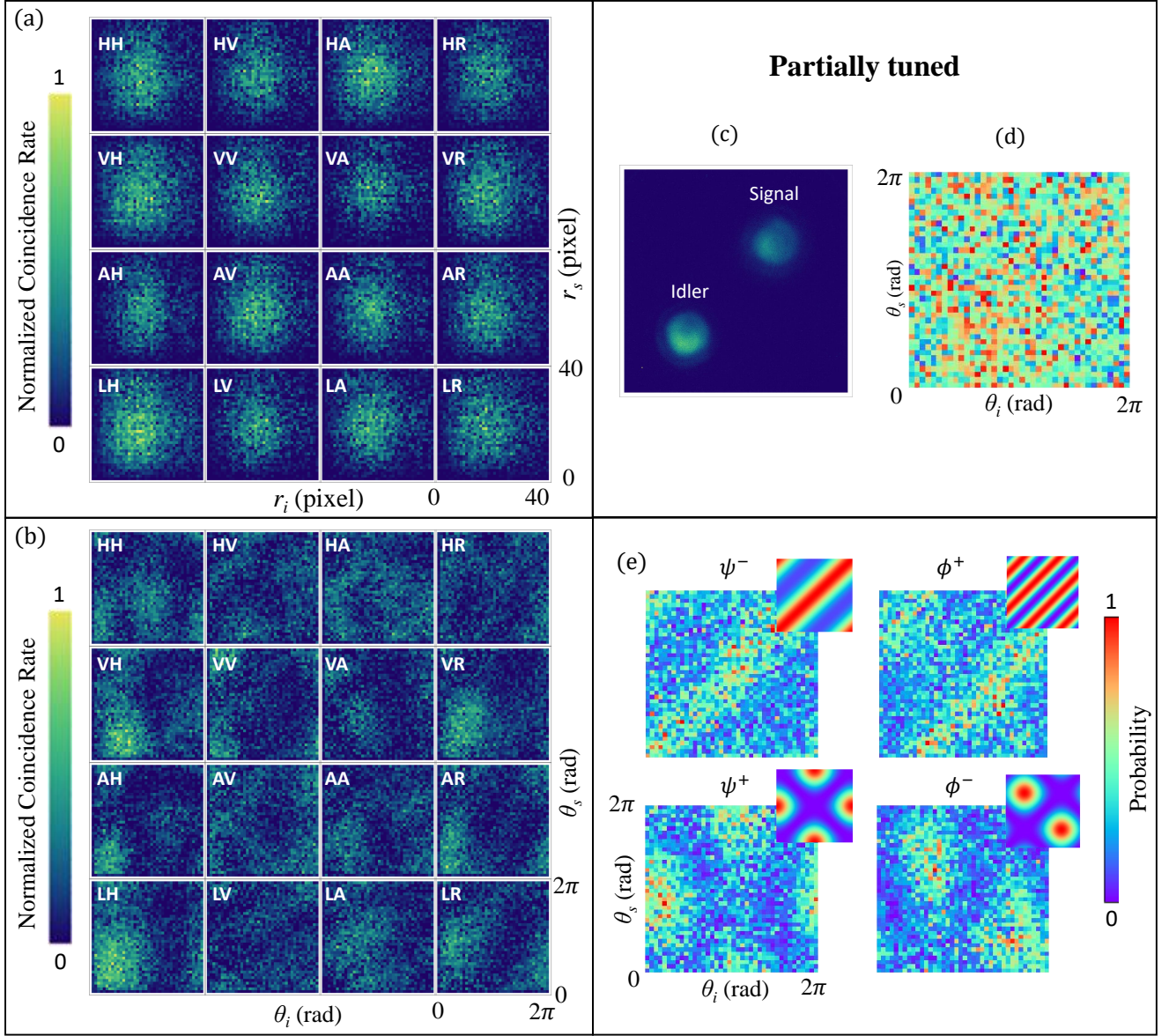


Figure S10. Measured spatial correlations and entanglement characterization for bi-photon with spatially varying polarization states generated via two q -plates. (a)-(b) Two-photon spatial correlations between two entangled vector beams measured, in the radial and azimuthal DOF respectively, from 16 different polarization measurements. Two partially tuned q -plates ($\delta_s = \delta_i = \pi/2$) with topological charges $q_i = -1/2$ and $q_s = -1/2$ are used to generate the entangled vector vortex photons. (c) Continuous exposure images recorded on the camera. (d) The concurrence of the entangled state and the average concurrence is measured to be 0.547 ± 0.061 . (e) Reconstructed probabilities for the four Bell states $\{|\psi^+\rangle, |\psi^-\rangle, |\phi^+\rangle, |\phi^-\rangle\}$. The insets are the respective theoretical probabilities.

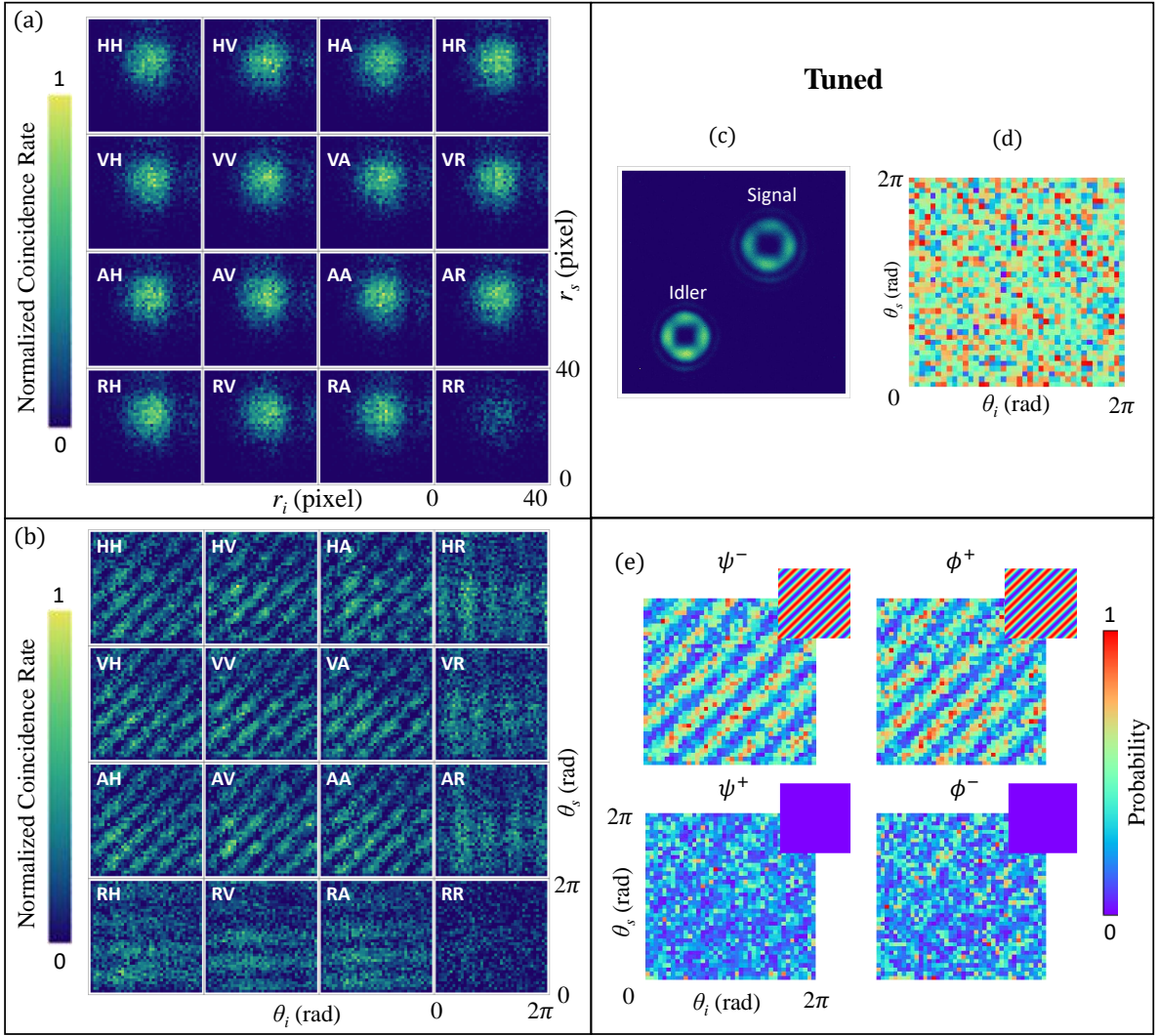


Figure S11. Measured spatial correlations and entanglement characterization for bi-photon with spatially varying polarization states generated via two q -plates. (a)-(b) Two-photon spatial correlations between two entangled vector beams measured, in the radial and azimuthal DOF respectively, from 16 different polarization measurements. Two tuned q -plates ($\delta_s = \delta_i = \pi$) with topological charges $q_i = 1$ and $q_s = 1$ are used to generate the entangled vector vortex photons. (c) Continuous exposure images recorded on the camera. (d) The concurrence of the entangled state and the average concurrence is measured to be 0.549 ± 0.032 . (e) Reconstructed probabilities for the four Bell states $\{|\psi^+\rangle, |\psi^-\rangle, |\phi^+\rangle, |\phi^-\rangle\}$. The insets are the respective theoretical probabilities.

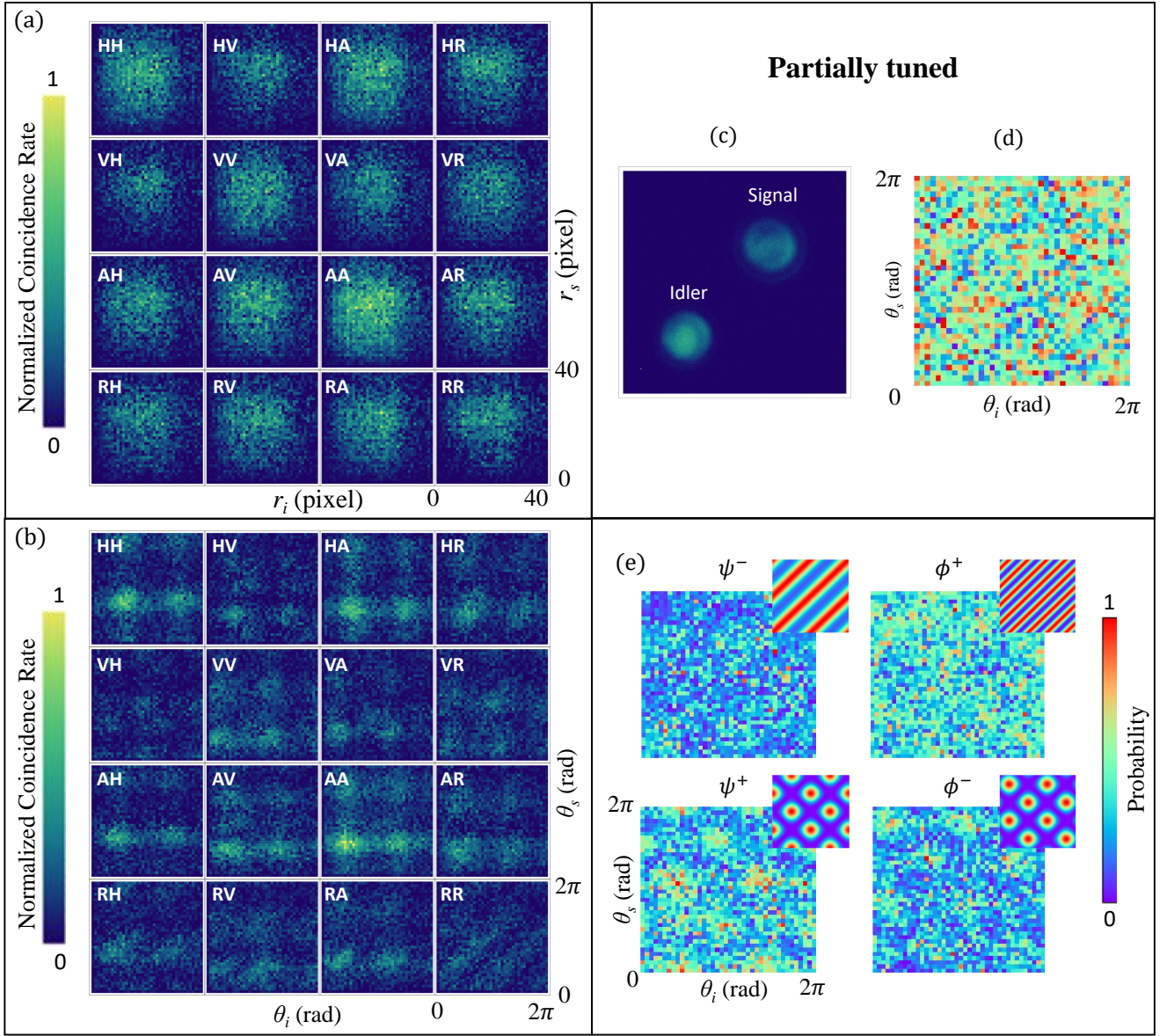


Figure S12. Measured spatial correlations and entanglement characterization for bi-photon with spatially varying polarization states generated via two q -plates. (a)-(b) Two-photon spatial correlations between two entangled vector beams measured, in the radial and azimuthal DOF respectively, from 16 different polarization measurements. Two partially tuned q -plates ($\delta_s = \delta_i = \pi/2$) with topological charges $q_i = 1$ and $q_s = 1$ are used to generate the entangled vector vortex photons. (c) Continuous exposure images recorded on the camera. (d) The concurrence of the entangled state and the average concurrence is measured to be 0.518 ± 0.013 . (e) Reconstructed probabilities for the four Bell states $\{|\psi^+\rangle, |\psi^-\rangle, |\phi^+\rangle, |\phi^-\rangle\}$. The insets are the respective theoretical probabilities.